



**HAL**  
open science

## Analysis of multifunctional oxycarbide and oxynitride thin films by modulated IR radiometry

Radiometry J Gibkes, F Vaz, a C Fernandes, P Carvalho, F Macedo, R T Faria, P Kijamnajsuk, J Pelzl, B K Bein

### ► To cite this version:

Radiometry J Gibkes, F Vaz, a C Fernandes, P Carvalho, F Macedo, et al.. Analysis of multifunctional oxycarbide and oxynitride thin films by modulated IR radiometry. *Journal of Physics D: Applied Physics*, 2010, 43 (39), pp.395301. 10.1088/0022-3727/43/39/395301 . hal-00569718

**HAL Id: hal-00569718**

**<https://hal.science/hal-00569718>**

Submitted on 25 Feb 2011

**HAL** is a multi-disciplinary open access archive for the deposit and dissemination of scientific research documents, whether they are published or not. The documents may come from teaching and research institutions in France or abroad, or from public or private research centers.

L'archive ouverte pluridisciplinaire **HAL**, est destinée au dépôt et à la diffusion de documents scientifiques de niveau recherche, publiés ou non, émanant des établissements d'enseignement et de recherche français ou étrangers, des laboratoires publics ou privés.

## Analysis of Multifunctional Oxycarbide and Oxynitride Thin Films by Modulated IR Radiometry

J. Gibkes<sup>1,2</sup>, F. Vaz<sup>3</sup>, A.C. Fernandes<sup>3</sup>, P. Carvalho<sup>3</sup>, F. Macedo<sup>4</sup>, R.T. Faria Jr.<sup>4,5</sup>,  
P. Kijamnajsuk<sup>2,6</sup>, J. Pelzl<sup>2</sup>, B.K. Bein<sup>2</sup>

<sup>1</sup>Georg Agricola University of Applied Sciences, D-44787 Bochum, Germany

<sup>2</sup>Solid State Spectroscopy, Physics & Astronomy, Ruhr-University Bochum, D-44780 Bochum, Germany

<sup>3</sup>Center of Physics, University of Minho, Campus de Azurém, 4800-058 Guimarães, Portugal

<sup>4</sup>Center of Physics, University of Minho, Campus de Gualtar, 4710-057 Braga, Portugal

<sup>5</sup>Physics Sciences Laboratory, Norte Fluminense State University, 28013-602 Campos, RJ, Brazil

<sup>6</sup>Physics Department, Faculty of Science, Kasetsart University, 10900 Bangkok, Thailand  
[fvaz@fisica@uminho.pt](mailto:fvaz@fisica@uminho.pt)      [fmacedo@fisica.uminho.pt](mailto:fmacedo@fisica.uminho.pt)

### Abstract

Multifunctional coatings consisting of transition metal oxycarbides and oxynitrides deposited by physical vapour deposition techniques on tool steel are analyzed in this work by means of Modulated IR Radiometry, a non-contact non-destructive thermal wave measurement technique, with respect to the thermal transport properties relevant for time-dependent surface heating processes of coating-substrate systems. In order to interpret the measured data quantitatively, an inverse solution of the two-layer thermal wave problem is applied, which relies on the thermal wave phase lag data measured as a function of modulation frequency of the periodically modulated laser beam heating intensity. Based on these measurements and their quantitative interpretation, correlations between the thermal transport properties of the coatings and their deposition conditions have been found, which can be used to monitor deposition processes. For a second objective of this work, namely to determine the film thickness by means of Modulated IR Radiometry, different sets of thin films of approximately constant thermal transport properties, but differing film thickness, have been measured. To discuss the limitations and error limits of these non-contact non-destructive measurements of the coating thickness, the results obtained by Modulated IR Radiometry are compared with the coating thickness determined by destructive measurements.

**Keywords:** Coatings, deposition control, Modulated IR Radiometry, thermal properties, thickness.

### 1. Introduction

A significant amount of work on multifunctional nano-structured coatings deposited by Physical Vapour Deposition (PVD) techniques including that of magnetron sputtering has been done during recent years, and various coating systems have been developed for the most different applications. A large number of such coating systems has been developed, to be used as protection in severe environments involving friction wear, corrosion, and oxidization at high temperatures. For these applications, different types of hard, tough, low-frictional, and thermally stable coatings have been synthesized. The motivation for these research studies was mainly related to the effects that the composition and structural features can have on the properties and performance of multifunctional films. As a result of an appropriate selection of coating methods and materials, one can get simultaneously good mechanical-tribological protection of the coated parts and a wide range of surface properties, including electrical and optical properties. Among the attempts to prepare such protective multifunctional thin films, transition-metal carbides ( $\text{MeC}_x$ ) and nitrides ( $\text{MeN}_x$ ) proved to be very attractive base

materials due to the combination of high hardness, high melting points [1], and good wear and corrosion resistance [2]. These materials - with only a very small band gap or without band gap - usually have optical and electrical properties of low variability, with a low variation of the refraction index and with electrically roughly metallic behavior. Adding, however, only small amounts of a third element to these carbides and nitrides, such as e.g. oxygen, structural changes can occur, offering the possibility to tailor materials of a much wider range of desired properties. In the case of oxygen addition, this multi-functionality is the result of a synergy - on the nano-scale level - of the beneficial properties of metal oxides (optical and electrical properties) and carbides/nitrides (electrical, mechanical, and tribological properties) on the synthesized oxycarbide and oxynitride coatings. In fact, merging the two classes of materials (oxides and carbides/nitrides) offers the possibility to produce new materials of a yet unexplored functionality. Changing the oxygen-to-carbon/nitrogen ratio - spanning the widest compositional range possible - will result in a progressive change of the materials properties between those of ionic metal oxides and those of covalent carbides/nitrides, with the consequent variation of all materials properties.

Hard coatings of transition metal oxynitrides and oxycarbides ( $\text{MeO}_x\text{N}_y$ ,  $\text{MeC}_x\text{O}_y$ ), deposited by vapour deposition techniques, are applied on industrial devices and components to increase their lifetime and performance, mainly due to such properties as high hardness, wear resistance, and chemical stability. Although in general such coating systems are successfully applied in cutting, casting, or hot forming, localized heat sources and high temperatures can give rise to micro-structural changes, which can affect the application-oriented properties and can lead to premature failures of the coatings. Thus, detailed knowledge about the coatings' thermal transport properties and their behavior under transient heat loads is essential for the successful development and application of such coatings, and information on the correlation between the coating deposition conditions and the resulting thermal transport properties may be most useful for the development of new coatings. To this finality Modulated IR Radiometry (MIRR) has been applied, which due to the non-contact, non-destructive excitation and detection of small-amplitude temperature oscillations, so-called *thermal waves*, is most appropriate for depth-resolved measurements of the thermal transport properties of layer systems. For a second major objective of this work, namely to determine the film thickness by means of Modulated IR Radiometry, various sets of thin films have been measured and the results obtained by MIRR have been compared with the coating thickness determined by destructive measurements, in order to study the reliability and the limitations of the non-destructive depth-resolved measurement method.

In Section 2 experimental details related to the films' production and their basic chemical and structural characterization are given, whereas a general description of Modulated IR Radiometry is given in Sect. 3, including the measurement technique and details of the quantitative interpretation based on the inverse solution of the two-layer thermal wave problem. In Sect. 4, several correlations between the measured thermal parameters of ZrON thin films and the deposition conditions are established, and in Sect. 5 the method to determine the coating thickness by means of Modulated IR Radiometry is presented and discussed with respect to principal limitations and error limits.

## **2. Details of Thin Film Deposition and Characterization**

For the present work, zirconium oxynitride ( $\text{ZrO}_x\text{N}_y$ ) and titanium oxycarbide ( $\text{TiC}_x\text{O}_y$ ) thin films have been deposited by reactive DC magnetron sputtering on high speed steel (AISI M2) substrates, using a laboratory-size deposition system. The films were prepared with the substrate holder positioned at 70 mm from the target, using a DC current density of  $100 \text{ A}\cdot\text{m}^{-2}$  in both the Zr and Ti targets. The Ti target had 12 cylindrical carbon pellets (10 mm diameter) placed in the preferential eroded zone, serving as C source in the preparation of the  $\text{TiC}_x\text{O}_y$

thin films. The targets had a surface dimension of  $200 \times 100 \text{ mm}^2$ , about 6 mm thick, and a 99.6 at. % purity. Gas atmospheres composed of argon and a nitrogen+oxygen reactive mixture (95 %  $\text{N}_2$  + 5 %  $\text{O}_2$ , using flows varying from 4 to 17.5 sccm, and partial pressures varying between  $3.2 \times 10^{-2}$  and  $1.6 \times 10^{-1}$  Pa) were used for the deposition of the oxynitride films, while an argon-oxygen atmosphere ( $\text{O}_2$  flow rate varying from 0.5 to 10 sccm, corresponding to a partial pressure variation from  $7.8 \times 10^{-3}$  to  $8.6 \times 10^{-2}$  Pa) was used for the preparation of the oxycarbide films. The argon flow was kept constant at 60 sccm in all depositions, and the working gas pressure changed only slightly between about 0.4 and 0.5 Pa. The effective pumping speed was adjusted to  $356 \text{ L s}^{-1}$ . The deposition temperature was set to be close to  $200 \text{ }^\circ\text{C}$  (using a heating resistance positioned at 80 mm from the substrate holder and a thermocouple placed close to the surface of the substrate holder on the plasma side to measure the temperature immediately after stopping the discharge).

The atomic composition of the as-deposited coatings was measured by Rutherford Backscattering Spectroscopy (RBS) using a 2 MeV  $\text{He}^+$  beam as well as 1.4 and 2 MeV proton beams, to increase the accuracy in the oxygen signals [3,4]. The structure and the phase distribution of the coatings were analyzed by X-ray diffraction (XRD), using a Philips PW 1710 diffractometer (Cu-K $\alpha$  radiation) operating in a Bragg–Brentano configuration. The XRD patterns, assumed to be Voigt functions, were deconvoluted, yielding the peak position, the integrated intensity, and the integrated width (IntW). Based on these parameters the fundamental structural parameters of the coatings were determined, including the interplanar distance, the preferential orientation, and the grain sizes. Morphological features of the samples (plane view micrographs as well as cross-section observations) were probed by scanning electron microscopy (SEM), carried out with a Jeol JSM 6301F microscope operating at 15 keV. Ball cratering tests, obtained with the help of a CSM CALOTEST apparatus [5], were used to measure the thickness of the coatings.

### 3. Basics of Modulated IR Radiometry – Measurement Technique and Signal Interpretation

Modulated IR Radiometry (MIRR), a non-destructive measurement technique based on the excitation of thermal waves by intensity-modulated laser beam heating and IR detection of the resulting thermal wave response, has been applied to determine the thermal transport parameters of the thin films, namely the (thermal) effusivity, the thermal diffusion time, and other thermal parameters which are relevant for time-dependent surface heating processes of coatings, as well as in other research fields [6].

The measurement system used for the excitation and non-contact detection of thermal waves (Fig. 1) consists of four main components: - (1) The beam of an Argon ion laser (Spectra Physics, Series 2000), with the wavelength given by  $\lambda = 514 \text{ nm}$  and its intensity periodically modulated by means of an acousto-optical modulator (ISOMET Corp. 1205C-2), is used to excite small periodical temperature oscillations, so called *thermal waves*, at the sample surface. The heating modulation frequency can be varied in the range from 0.03 Hz to 100 kHz, allowing depth-resolved thermal measurements in the range from about 2 mm to thin films of less than  $1 \text{ }\mu\text{m}$  beneath the surface heating spot of a diameter of about 3 mm. - (2) IR optics of short focussing length of about 15 cm, consisting of two large-diameter Barium-fluoride lenses (10 cm) and an IR filter limiting the detectable IR wavelength interval to 2 - 12  $\mu\text{m}$ , are used to focus the IR radiation, emitted by the sample surface within a diameter of about 1.4 mm, on a liquid-nitrogen cooled Mercury-Cadmium-Telluride (MCT) IR detector (Judson-Infrared, JD15-D12). - (3) A two-phase Lock-in amplifier (Stanford 830 DSP) is used to filter the small periodical variations of the detected IR emission related to the temperature oscillations of the sample - at the modulation frequency of excitation - from the high radiation and temperature background of more than 300 K. The in-phase and out-of-

phase components of the modulated IR signal supplied by the two-phase Lock-in amplifier give information on the thermal wave's amplitude  $A$  and its phase lag  $\Phi$  relative to the modulated excitation. - (4) The whole measurement process is controlled by a computer, which simultaneously is used to store the amplitude and phase lag data measured as a function of the heating modulation frequency  $f$ .

The detection limit of the measurement system (Fig. 1) for thermal waves mainly depends on the noise of the incident radiation and on the noise produced by the IR detector itself and by the electronic system following the detector. The noise related to the detector and to the electronic system, known as  $1/f$  - noise and relevant only at low modulation frequencies, can be minimized using a cooled detector and an optimal electronic adaptation between detector and pre-amplifier. In principle, the radiation incident on the IR detector is affected by two types of fluctuations: - Fluctuations of the thermal wave signal and fluctuations of the IR background radiation. Using a Lock-in amplifier, fluctuations of the resulting thermal-wave signal have been found to be negligible due to the Lock-in-controlled repeated measurement and signal filtering of the thermal wave response at constant modulation frequencies, and thus the incoherent IR background fluctuations have been found to represent the main limitation for Modulated IR Radiometry [7]. In systematic studies on the detection limits of the described detection system thermal wave amplitudes above about 44  $\mu\text{K}$ , 15  $\mu\text{K}$ , and 9  $\mu\text{K}$  have successfully been detected in a closed high-temperature cell at average sample background temperatures of 300 K, 400K, and 500 K, respectively.

Based on the reflection configuration of thermal waves, with the excitation and the detection of the thermal wave response taking place at the coated surface of the samples (Fig. 1), depth resolved measurements of the thermal properties of layer systems, consisting of thin films and coatings on thermally thick substrates can be done [8]. In order to interpret the signals measured for layer systems quantitatively, these have to be calibrated with the help of thermal wave signals measured for homogeneous opaque reference samples of smooth surface under the same conditions of heating and detection. The frequency characteristics of the various components of the measurement system, e.g. of IR detector and pre-amplifier, are eliminated by this normalization or calibration process.

### 3.1. Theoretical Description of the Measured Amplitude and Phase Signals

Assuming a large heating spot diameter and one-dimensional heat propagation, the thermal waves excited at the smooth surface of a coating, which is opaque at the wavelength of the heating laser beam, are described by

$$\delta T_c(x_c, t) = \frac{\eta_c I_0}{2k_c \sigma_c} \frac{1 + R_{cb} \exp[-2\sigma_c(d_c - x_c)]}{1 - R_{cb} \exp(-2\sigma_c d_c)} \exp(-\sigma_c x_c + i2\pi f t) \quad (1)$$

Here,  $\eta_c$  is the coating's photothermal efficiency describing the absorbed part of the incident laser beam intensity  $I_0$ ,  $d_c$  the coating thickness,  $x_c$  the distance beneath the coating surface, and  $t$  the time.  $R_{cb}$  is the thermal reflection coefficient [9] at the interface coating - substrate,

$$R_{cb} = -[1 - (e_c / e_b)] / [1 + (e_c / e_b)] \quad (2)$$

The quantity  $e_{c,b} = \sqrt{(k\rho c)_{c,b}}$  is the thermal effusivity of the coating (c) and substrate (b), respectively, with  $k$  the thermal conductivity,  $\rho$  the mass density, and  $c$  the specific heat capacity. The complex quantity

$$\sigma_c = (1 + i)\sqrt{(\pi f) / \alpha_c} \quad (3)$$

is the thermal wave vector, with  $\alpha_c = k_c / (\rho_c c_c)$  the thermal diffusivity of the coating and  $f$  the heating modulation frequency of the laser beam intensity. The quantity  $i$  in equ.(1) and (3) is the complex unity, which serves to describe the thermal wave's phase lag relative to the phase

of the heating modulation. Considering a coating which is opaque both in the IR spectral range and in the visible spectrum, the detected modulated IR signal can be described by

$$\delta M_c(T_c, f, t) = \gamma_D(T_c) \varepsilon_c(T_c) 4\sigma_{SB} T_c^3 \cdot \delta T_c(x_c=0, t) = \gamma_D(T_c) \varepsilon_c(T_c) 4\sigma_{SB} T_c^3 \frac{\eta_c I_0}{2k_c \sigma_c} \frac{1 + R_{cb} \exp(-2\sigma_c d_c)}{1 - R_{cb} \exp(-2\sigma_c d_c)} \exp(i2\pi f t) \quad (4)$$

with  $\varepsilon_c(T_c)$  the effective emissivity of the coating in the detected IR wavelength interval,  $\sigma_{SB}$  Stefan-Boltzmann's constant, and  $T_c$  the time-averaged surface temperature of the coating. The quantity  $\gamma_D(T_c)$  is the detection efficiency for modulated IR radiation, depending on Planck's radiation law and the technical parameters of the IR focusing and detection system [7]. Using a two-phase Lock-in amplifier to amplify and filter the small periodical variations of the IR emission related to the thermal waves from the IR background radiation, the in-phase and out-of-phase contributions  $[A \cdot \sin \Phi(f)]$  and  $[A \cdot \cos \Phi(f)]$  of the modulated IR signals relative to the intensity-modulation of the heating laser beam are registered and are used to calculate the phase lag signals  $\tan \Phi(f) = [A \cdot \sin \Phi(f)] / [A \cdot \cos \Phi(f)]$  and the amplitude signals  $S(f) = \sqrt{[A \cdot \sin \Phi(f)]^2 + [A \cdot \cos \Phi(f)]^2}$  of the thermal waves. Based on equ.(4), the modulated IR phase lag signal for an opaque coating is described by

$$\tan \Phi_c(f) = -\frac{1 + 2R_{cb} \exp(-2\sqrt{\pi f \tau_c}) \sin(2\sqrt{\pi f \tau_c}) - R_{cb}^2 \exp(-4\sqrt{\pi f \tau_c})}{1 - 2R_{cb} \exp(-2\sqrt{\pi f \tau_c}) \sin(2\sqrt{\pi f \tau_c}) - R_{cb}^2 \exp(-4\sqrt{\pi f \tau_c})} \quad (5)$$

with the thermal diffusion time of the coating given by

$$\tau_c = d_c^2 / \alpha_c \quad (6)$$

For the quantitative interpretation, the modulated IR signals measured for a two-layer system of differing thermal transport properties are calibrated with the help of reference signals measured for a homogeneous opaque solid of smooth surface. Based on the assumption  $e_r = e_c = e_b$  and  $R_{cb} = 0$  (equ. 2), the amplitude and phase lag signals of the homogeneous reference are described by

$$\delta M_r(T_r, f, t) = \gamma_D(T_r) \varepsilon_r(T_r) \cdot 4\sigma_{SB} T_r^3 \cdot \frac{\eta_r I_0}{2k_r \sigma_r} \exp(i2\pi f t) \quad (4a)$$

$$\tan \Phi_r(f) = -1 \quad (5a)$$

In order to compare the measured signals with the theoretical approximations, the amplitudes and phases are represented in the inverse calibrated form

$$S_n^{-1}(f^{-1/2}) = \frac{\delta M_r(f)}{\delta M_c(f)} = \frac{\gamma_D(T_r) \varepsilon_r(T_r) T_r^3 \eta_r}{\gamma_D(T_c) \varepsilon_c(T_c) T_c^3 \eta_c} \frac{e_c}{e_r} \frac{1 - 2R_{cb} \exp(-2\sqrt{\pi f \tau_c}) \cos(2\sqrt{\pi f \tau_c}) + R_{cb}^2 \exp(-4\sqrt{\pi f \tau_c})}{\sqrt{1 - 2R_{cb}^2 \exp(-4\sqrt{\pi f \tau_c}) \cos(4\sqrt{\pi f \tau_c}) + R_{cb}^4 \exp(-8\sqrt{\pi f \tau_c})}} \quad (7)$$

$$\tan \Phi_n(f) = \tan[\Phi_r(f) - \Phi_c(f)] = \frac{\tan \Phi_r - \tan \Phi_c}{1 + \tan \Phi_r \tan \Phi_c} = \frac{2R_{cb} \exp(-2\sqrt{\pi f \tau_c}) \sin(2\sqrt{\pi f \tau_c})}{1 - [R_{cb} \exp(-2\sqrt{\pi f \tau_c})]^2} \quad (8)$$

This has the advantage that the inverse calibrated amplitudes (7) provide a visual impression of the effusivity depth profile (Fig. 2): - At high heating modulation frequencies, corresponding to short thermal wave penetration depths  $x_{th} \propto \mu_{th} = \sqrt{\alpha / (\pi f)} \Big|_{f \rightarrow \infty} \rightarrow 0$ , the

inverse calibrated amplitudes

$$S_n^{-1}(f) \Big|_{f \rightarrow \infty} = \frac{\gamma_D(T_r)}{\gamma_D(T_c)} \cdot \frac{\varepsilon_r(T_r)}{\varepsilon_c(T_c)} \cdot \frac{T_r^3}{T_c^3} \cdot \frac{\eta_r}{\eta_c} \cdot \frac{e_c}{e_r} \quad (7a)$$

are proportional to the effusivity  $e_c$  of the coating, and at low heating modulation frequencies, corresponding to large penetration depths,  $x_{th} \propto \mu_{th} = \sqrt{\alpha/(\pi f)} \Big|_{f \rightarrow 0} \rightarrow \infty$ , the inverse calibrated amplitudes are proportional to the effusivity  $e_b$  of the substrate,

$$S_n^{-1}(f) \Big|_{f \rightarrow 0} = \frac{\gamma_D(T_r) \cdot \varepsilon_r(T_r) \cdot T_r^3 \cdot \eta_r \cdot e_c \cdot (1 - 2R_{cb} + R_{cb}^2)}{\gamma_D(T_c) \cdot \varepsilon_c(T_c) \cdot T_c^3 \cdot \eta_c \cdot e_r \cdot \sqrt{1 - 2R_{cb}^2 + R_{cb}^4}} = \frac{\gamma_D(T_r) \cdot \varepsilon_r(T_r) \cdot T_r^3 \cdot \eta_r \cdot e_b}{\gamma_D(T_c) \cdot \varepsilon_c(T_c) \cdot T_c^3 \cdot \eta_c \cdot e_r} \quad (7b)$$

Figure 2 shows the inverse calibrated modulated IR amplitudes measured for some ZrON sputter-deposited coatings on tool steel, selected according to their specific deposition conditions, namely the amount of the used reactive gas flow (a mixture of 95 % N<sub>2</sub> + 5 % O<sub>2</sub>): - The coatings ZrON1 and ZrON2 were prepared with reactive gas flows of 8.5 and 9 sccm, respectively, keeping constant all other deposition parameters (dc current density in the target, grounded condition of the substrates, working gas - argon - flow, and no external heating). The two coatings ZrON3 and ZrON4 were prepared with reactive gas flows of 16 and 17.5 sccm, keeping again constant all other deposition parameters, described in more detail in ref. [3].

As can be seen on the left hand side of Fig. 2, the effusivity of the coatings (7a) is smaller than the effusivity of the substrate (7b) on the right hand side of Fig. 2,  $e_c < e_b$ . On the other hand, the differences of the inverse calibrated amplitude signals  $S_n^{-1} = S_r/S_c$  on the right hand side of Fig. 2, where the properties of the substrate are measured, indicate that the combined parameters  $[\gamma_D(T_c)\varepsilon_c(T_c)T_c^3\eta_c]$  differ considerably for the various coatings, mainly due to differences in the optical coating parameters  $\varepsilon_c$  and  $\eta_c$ . For the quantitative interpretation it is thus preferable to consider the inverse calibrated phase lag signals, which according to equ. (8) only depend on two combined thermal parameters, namely the coating's thermal diffusion time (6) and the thermal reflection coefficient  $R_{cb}$  (2), whereas the inverse calibrated amplitude signals (7) additionally depend on the ratio of the effusivities coating-to-reference material,  $(e_c/e_r)$ , and on a further parameter  $[\gamma_D(T_r)\varepsilon_r(T_r)T_r^3\eta_r]/[\gamma_D(T_c)\varepsilon_c(T_c)T_c^3\eta_c]$  combining the device-dependent detection efficiency, the emissivity, the time-averaged surface temperature, and the photothermal efficiency of both the reference material and of the coating.

In Fig. 2 it is also interesting to see that the inverse calibrated amplitudes show a continuous transition between the effusivities  $e_c$  of the coatings at small penetration depths and the effusivity  $e_b$  of the substrate at large penetration depths and that there is no evidence for any thermal contact resistance between the coatings and the substrate. This is due to the fact, that - before coating deposition - the surfaces of the substrates had been cleaned by a plasma treatment during 20 min consisting of Argon ion bombardment carried out at an Ar flow of 60 sccm (a partial pressure of  $3 \times 10^{-3}$  mbar), and applying a pulsed DC current of 0.5 A ( $f_{pulse} = 200$  kHz and a duty cycle of 51 %). This plasma treatment was performed in order to achieve two major objectives: - (1) To eliminate, respectively to reduce the oxide contamination layer commonly present at metal-like surfaces such as high speed steel (AISI M2) and - (2) to create a micro-roughness-increased effective surface area at the substrate surface offering enhanced adhesion for the coating. The resulting homogeneous and clean substrate surface contributes to the perfect thermal transition between coatings and substrates, confirmed by the results of Modulated IR Radiometry (Fig. 2).

Apart from the in general continuous behavior of the inverse calibrated measured signal amplitudes, two types of fluctuations, already discussed in Sect. 3, can be identified in Fig. 2, namely  $1/f$ -noise at lower modulation frequencies  $1 \leq (f/\text{Hz}) \leq 100$ , affecting the inverse calibrated amplitudes of the coatings ZrON1 and ZrON2 at larger thermal penetration depths  $x_{th} \propto \mu_{th} = \sqrt{\alpha/(\pi f)} \propto (f/\text{Hz})^{-1/2} \geq 0.1$ , and IR background fluctuations at high modulation frequencies affecting the inverse calibrated amplitudes of the coating ZrON4 in the limit of the shorter penetration depths,  $(f/\text{Hz})^{-1/2} \leq 0.003$ .

The inverse calibrated modulated IR phases (Fig. 3) measured for the sputter-deposited ZrON coatings on tool steel show pronounced relative minima in the intermediate range of modulation frequencies,  $45 < (f/\text{Hz})^{1/2} < 75$ , which can well be approximated by two-layer solutions, whereas at higher modulation frequencies,  $(f/\text{Hz})^{1/2} > 150$ , larger deviations from the two-layer approximations can be observed. In general, the range of the intermediate modulation frequencies with the relative minima of the inverse calibrated phase signals gives information on the thermal transport properties of the coating as a whole, whereas the range of the higher modulation frequencies can give information on the semi-transparency of the coatings or on a three-layer structure, with a very thin layer just at the surface of the coating of reduced effusivity,  $e_s < e_c$ , related e.g. to surface roughness [10,11].

In fact, and as described in more detail in Sect. 4, the coatings ZrON1 and ZrON2 are metal-like coatings with a cubic-type structure, whereas the coatings ZrON3 and ZrON4 have a different crystalline structure characterized by a mixture of two electrically insulating structures: An orthorhombic nitride structure and a cubic oxynitride structure [3].

These differences of composition and structure, which affect all film properties [3,4], are found in the range of intermediate and higher modulation frequencies of the inverse calibrated modulated IR phases (Fig.3): - At intermediate modulation frequencies,  $50 < (f/\text{Hz})^{1/2} < 65$ , the coatings ZrON1 (o) and ZrON2 ( $\Delta$ ) exhibit smaller negative values of the measured relative minima,  $\Phi_{n \text{ extr}} = -16.3$  deg, corresponding to higher values of the coatings' effusivity, whereas the coatings ZrON3 ( $\square$ ) and ZrON4 (+) show relative minima of about  $-20 \text{ deg} < \Phi_{n \text{ min}} < -21.5$  deg, corresponding to smaller effusivity values of the coating. In the range of the higher modulation frequencies,  $(f/\text{Hz})^{1/2} > 150$ , the inverse calibrated phases measured for the two coatings ZrON3 ( $\square$ ) and ZrON4 (+) considerably exceed the zero-line ( $\Phi_n = 0$  deg), showing a behavior which is characteristic for semi-transparent coatings, as observed in fact for these two films in optical measurements carried out by UV-Vis spectrophotometry [3,4]. On the other hand, the inverse calibrated phases, measured for the two coatings ZrON1 (o) and ZrON2 ( $\Delta$ ) at higher modulation, deviate from the two-layer model to lower values. This behaviour, which is characteristic for a three-layer structure with a thin surface on top of the coating of reduced thermal effusivity,  $e_s < e_c$ , can be explained for the two coatings ZrON1 and ZrON2 by very thin oxide contamination layers just at the surface [4].

At very low modulation frequencies,  $(f/\text{Hz})^{1/2} < 25$ , corresponding to larger penetration depths, the inverse calibrated modulated IR phases (Fig. 3) can also give information on the effects of substrate treatment [8], bond layers between coating and substrate, and heat propagation inside the substrate [12]. Similar to the information obtained from the inverse calibrated modulated IR amplitudes (Fig. 2), Figure 3 also shows that there is no evidence for any thermal contact resistance between the coatings and the substrate.

### 3.2. Quantitative Interpretation of the Inverse Calibrated Phase Lag Signals

For the quantitative interpretation of the inverse calibrated measured phase lag signals, an inverse analytical solution of the two-layer thermal wave problem is used [13], which relies on the value measured as a function of heating modulation frequency for the relative extremum

$$\tan \Phi_n(f) \Big|_{f=f_{\text{extr}}} = \tan[\Phi_r(f) - \Phi_c(f)] \Big|_{f=f_{\text{extr}}} = \tan \Phi_{n \text{ extr}} = \frac{2R_{\text{cb}} \exp(-2\sqrt{\pi f_{\text{extr}}} \tau_c) \sin(2\sqrt{\pi f_{\text{extr}}} \tau_c)}{1 - [R_{\text{cb}} \exp(-2\sqrt{\pi f_{\text{extr}}} \tau_c)]^2} \quad (9)$$

and on the extremum condition, which has to be fulfilled simultaneously

$$\left. \frac{\partial \tan \Phi_n(f)}{\partial(\sqrt{f})} \right|_{f=f_{\text{extr}}} = \frac{4R_{\text{cb}}\sqrt{\pi\tau_c} \exp(-2\sqrt{\pi f\tau_c})}{[1-R_{\text{cb}}^2 \exp(-4\sqrt{\pi f\tau_c})]^2} \left\{ \begin{aligned} & [1-R_{\text{cb}}^2 \exp(-4\sqrt{\pi f\tau_c})] \cos(2\sqrt{\pi f\tau_c}) - \\ & - [1+R_{\text{cb}}^2 \exp(-4\sqrt{\pi f\tau_c})] \sin(2\sqrt{\pi f\tau_c}) \end{aligned} \right\} \Big|_{f=f_{\text{extr}}} = 0 \quad (10)$$

The extremum condition (10) can also be written as

$$\cos(2\sqrt{\pi f_{\text{extr}}\tau_c}) = \frac{[1+R_{\text{cb}}^2 \exp(-4\sqrt{\pi f_{\text{extr}}\tau_c})]}{[1-R_{\text{cb}}^2 \exp(-4\sqrt{\pi f_{\text{extr}}\tau_c})]} \sin(2\sqrt{\pi f_{\text{extr}}\tau_c}) \quad (11)$$

The two equations and conditions (9) and (11) are linearly independent and depend on the two measurable quantities  $\tan \Phi_{n \text{ extr}}$  and  $f_{\text{extr}}$ . On the other hand, the two equations (9) and (11) depend on the two coating parameters  $R_{\text{cb}}$  (2) and  $\tau_c$  (6). The inverse solutions of the two equations (9) and (11) for the thermal coating parameters  $R_{\text{cb}}$  and  $\tau_c$ , which have been found in analytical form [13],

$$R_{\text{cb}} = \pm \sqrt{\frac{1 - \tan\{0.5 \cdot \cos^{-1}[(\tan \Phi_{n \text{ extr}})^2]\}}{1 + \tan\{0.5 \cdot \cos^{-1}[(\tan \Phi_{n \text{ extr}})^2]\}}} \cdot \exp\{0.5 \cdot \cos^{-1}[(\tan \Phi_{n \text{ extr}})^2]\} \quad (12)$$

$$\tau_c = \frac{1}{16\pi f_{\text{extr}}} \{\cos^{-1}[(\tan \Phi_{n \text{ extr}})^2]\}^2 \quad (13)$$

allow to determine the thermal transport properties of the coating, when the relative extrema of the inverse calibrated phase lag signals have been measured, i.e. the value  $\Phi_{n \text{ extr}}$  of the inverse calibrated phase lag signals and the modulation frequency  $f_{\text{extr}}$  at the position of the relative extremum.

According to equ.(9), the sign for the solution of the *thermal reflection coefficient*  $R_{\text{cb}}$  (12) has to be chosen in agreement with the extremum measured for the inverse calibrated modulated phases. This means, for the coatings for which relative minima have been found in Fig.3, the negative sign has to be used in equ.(12). When on the other hand a relative maximum is measured for the inverse calibrated phase lag signals, the positive sign has to be used in equ.(12).

Based on the solution for the thermal reflection coefficient  $R_{\text{cb}}$  (12), the ratio of the effusivities coating-to-substrate can then be determined according to the inversion of equ.(2)

$$(e_c / e_b) = \sqrt{(k\rho c)_c} / \sqrt{(k\rho c)_b} = (1 + R_{\text{cb}}) / (1 - R_{\text{cb}}) \quad (14)$$

Following equ. (12) and (14), the ratio of the effusivities coating-to-substrate only depends on the absolute value of the measured relative phase extremum,  $|\tan \Phi_{n \text{ extr}}|$ , and is thus determined as mathematically unique solution. The thermal diffusion time (13), which depends on the heating modulation frequency  $f_{\text{extr}}$  and on the absolute value  $|\tan \Phi_{n \text{ extr}}|$  measured at the relative extremum, is also determined as mathematically unique solution.

A necessary condition for this direct and reliable determination of the coating's thermal parameters  $R_{\text{cb}}$ ,  $(e_c/e_b)$ , and  $\tau_c$ , is that the relative extrema of the inverse calibrated modulated IR phases are accessible to measurement. This may not always be the case, e.g. in the case of rather thin coatings, for which the relative extremum should be measured at very high modulation frequencies where the thermal wave detection [7] may already be affected by IR background fluctuations (Comp. Sect.5, Fig. 9). In photoacoustic thermal wave detection, the relative extrema may be disturbed in the neighborhood of the acoustic cell resonances and their multiples. In order to exclude such limitations imposed by the measurement technique, a Combined Transformation and Extremum Method [13] can be applied and the thermal coating parameters  $R_{\text{cb}}$ ,  $(e_c/e_b)$ , and  $\tau_c$  can then be determined from the modulated phase lag signals measured in the neighborhood of the relative extrema.

Based on the thermal coating parameters ( $e_c/e_b$ ) and  $\tau_c$ , directly determined as a function of the measured relative extremum of the inverse calibrated phase lag signals, two combined coating parameters, namely the *thickness specific thermal conductivity*

$$(k_c/d_c) = [(e_c/e_b)/\sqrt{\tau_c}] \cdot e_b \quad (15)$$

and the *surface area heat capacity*

$$[d_c(\rho c)_c] = [(e_c/e_b) \cdot \sqrt{\tau_c}] \cdot e_b \quad (16)$$

can be calculated, which serve to characterize and compare coatings deposited on the same substrate with respect to the heat transport properties across the coating or the heat insulation properties of the coating. These parameters can be considered as technologically relevant parameters e.g. for coated cutting tools [14], generally submitted to transient surface heating processes of limited duration, with the heat produced by friction just at the surface.

While the thermal diffusion time  $\tau_c = d_c^2/\alpha_c$  (6) is the relevant parameter for the heat propagation across a layer of constant thermal transport properties, the thermal effusivity is the relevant parameter for time-dependent heating or cooling processes of surfaces. This can be seen, when the surface temperature evolution is considered,

$$T_s(t) = \frac{1}{\sqrt{e_s \pi}} \int_0^t dt' \frac{F_s(t-t')}{\sqrt{t'}} \quad (17)$$

resulting as a function of the time-dependent heat flux  $F_s(t)$  absorbed at the surface of a semi-infinite solid of constant thermal properties [15]. The inverse solution of equ. (17), which describes the absorbed heat flux as a function of the measured time-dependent surface temperature  $T_s(t)$  [16]

$$F_s(t) = \frac{\sqrt{e_s}}{2\sqrt{\pi}} \left\{ \int_0^t dt' \frac{[T_s(t) - T_s(t')]}{(t-t')^{3/2}} + 2 \frac{[T_s(t) - T_s(t=0)]}{\sqrt{t}} \right\} \quad (18)$$

can be used in quantitative IR thermography [17,18] to determine the heat fluxes incident as a result of plasma-wall interactions on the limiter and divertor plates in nuclear fusion devices. The relevant thermophysical parameter both in equ.(17) and (18) is the effusivity, which on limiter and divertor plates in nuclear fusion devices may exhibit a two-layer structure due to plasma wall interactions [16], similar to coated surfaces with a smaller effusivity of the coating than of the substrate.

#### 4. Correlations between Deposition Conditions and Thermal Parameters, Measured by means of Modulated IR Radiometry for ZrON Thin Films

In this section, the most relevant correlations between the thermal coating parameters and the deposition conditions of a set of ZrON thin films on tool steel, produced as a function of increasing ( $N_2+O_2$ )-gas flow, are shown (Table 1).

In Fig. 4, the measured values  $\Phi_{n \text{ extr}}$  of the relative extrema of the inverse calibrated phase lag signals are presented as a function of the increasing ( $N_2+O_2$ )-gas flow, used for the deposition of this set of coatings. As can be seen in Fig. 3, the value of the relative extremum  $\Phi_{n \text{ extr}}$  is here a quantity directly accessible to measurement in the range of the intermediate modulation frequencies,  $45 < (f/\text{Hz})^{1/2} < 70$ , which gives information on the thermal reflection coefficient  $R_{cb}$  at the interface coating-substrate (12) and on the ratio of the effusivities ( $e_c/e_b$ ) coating-to-substrate (14). When the effusivity of the substrate material is known, or when the substrate material for a set of coatings is equal, the resulting effusivity values  $e_c$  of the coatings can thus be monitored with the help of the directly measurable relative phase lag extremum  $\Phi_{n \text{ extr}} = \Phi_r - \Phi_c$ .

As can be seen in Fig. 4, there is a general correlation between the values measured for the phase lag extrema and the gas mixture flow: - With increasing gas mixture flow the negative values of the phase lag extrema first increase, whereas for higher gas mixture flows, above about 15 sccm, the negative values of the phase lag extrema decrease again. Once the correlation between gas mixture flow and the values of the relative phase lag extrema has sufficiently been explored, it might thus be possible to monitor the deposition process with the help of the phase lag extrema measured by Modulated IR Radiometry.

In Figure 5 and 6, the main thermal coating parameters obtained by Modulated IR Radiometry, namely the ratio of the thermal effusivities coating-to-substrate (Fig. 5) and the thermal diffusivity of the coatings (Fig.6), are presented for the ZrON thin film system as a function of the atomic concentration ratio  $(C_N+C_O)/C_{Zr}$ . The ratio of the effusivities ( $e_c/e_b$ ), which according to equ.(12) and (14) only depends on the measured value of the phase lag extremum  $\Phi_{n \text{ extr}}$  is one of the thermal coating parameters directly measurable by Modulated IR Radiometry. The thermal diffusivity of the coating

$$\alpha_c = d_{\text{c micro}}^2 / \tau_c \quad (19)$$

has to be calculated from the thermal diffusion time (13), measured by Modulated IR Radiometry, and from the coating thickness, determined by independent measurements, e.g. by destructive microscopic measurements  $d_{\text{c micro}}$  [5].

Figure 5 shows that the effusivity ratio ( $e_c/e_b$ ) generally decreases with increasing nitrogen and oxygen content, whereas at higher values of the nitrogen and oxygen content,  $(C_N+C_O)/C_{Zr} > 1.4$ , the effusivity ratio ( $e_c/e_b$ ) seems to be nearly constant or slightly increasing again. The thermal diffusivity  $\alpha_c$ , on the other hand, shows a rather strong and continuous decrease with increasing nitrogen and oxygen content, both at low and high values of the nitrogen and oxygen content (Fig.6).

These general correlations of both the effusivity ratio ( $e_c/e_b$ ) and the thermal diffusivity  $\alpha_c$  with the atomic concentration ratio  $(C_N+C_O)/C_{Zr}$  are related to structural features [19], which considerably vary with the coatings' composition. In fact and in agreement with the two main compositional zones observed for these coatings [3], the structural analysis, carried out by XRD, reveals the existence of two structurally distinct types of films:

- In a first zone, corresponding to the films with the atomic concentration ratio  $(C_N+C_O)/C_{Zr}$  varying from about 0.8 to about 1.4, the films crystallized in a B1-NaCl crystal structure, typical for ZrN [3]. In addition, there is a progressive change in the preferential growth of the films from  $\langle 111 \rangle$  to  $\langle 200 \rangle$ . The films ZrON1 and ZrON2 (Fig. 2 and Fig. 3) are two examples of films of this Zone I.

- In Zone II, on the other hand, the X-ray diffractograms of the films with the concentration ratio  $(C_N+C_O)/C_{Zr} > 1.4$  suggest the development of an overstoichiometric nitride-type phase, which was identified to be similar to that of  $Zr_3N_4$ , where oxygen may have a kind of catalytic effect [3]. This change in crystalline structures evolves in Zone II to a mixture of that of an oxygen doped  $Zr_3N_4$ -type structure with a cubic  $\gamma$ - $Zr_2ON_2$  phase at the highest concentration ratios. The films ZrON3 and ZrON4 represent two examples of films of this Zone II, revealing the phase mixture [3].

Here it should be mentioned that the two pairs of coatings {ZrON1, ZrON2} and {ZrON3, ZrON4} are representative for a larger variety of coatings, which are analyzed here with respect to possible correlations between deposition conditions and effective thermal coating parameters (Table 1) and which have already been analyzed elsewhere [3] with respect to their elemental composition and structural features (crystalline phases, grain sizes, crystallinity, preferential growth, etc.). Detailed analysis, carried out by RBS, revealed that all coatings have a homogeneous in-depth composition, associated also with a homogeneous in-depth morphology, as revealed by the cross-section analysis carried out by SEM. The films

have columnar-like growth, without abrupt changes in the columns' growth and width, and the quantitative interpretation based on the two-layer model and the relative extrema at the intermediate modulation frequencies,  $45 < (f/\text{Hz})^{1/2} < 70$ , thus should give reliable thermal coating parameters.

Regarding the thermal properties, one can see that the thin films revealing the fcc ZrN-type growth (Zone I) [3], have got higher values for both the effusivity ratios in Fig. 5,  $(e_c/e_b) > 0.32$ , and the thermal diffusivity in Fig. 6,  $\alpha_c > 8 \cdot 10^{-7} \text{ m}^2/\text{s}$ , confirming thus direct correlations between composition, structural features, and the thermal transport properties.

In contrast to the effusivity of the coatings (Fig. 5) and in contrast to the thermal diffusivity of the coatings (Fig. 6), which decreases nearly continuously as a function of the atomic concentration ratio  $(C_N+C_O)/C_{Zr}$ , the combined thermal parameter  $[(e_c/e_b) \cdot \sqrt{\tau_c}] \propto [d_c(\rho \cdot c)_c]$  decreases with the gas mixture flow in Zone I, whereas it slightly increases in Zone II (Fig. 7). This special behavior of the *surface area heat capacity*  $[d_c(\rho \cdot c)_c]$  correlates with the change in the crystalline structure, when passing from the Zone I to the Zone II coatings.

This sensitivity of the *surface area heat capacity*  $[d_c(\rho \cdot c)_c]$  with respect to differences of the crystalline structure is specially important for two reasons: - (i) Based on this combined parameter, the Zone I and Zone II and the correlated changes in crystalline structure can be distinguished, whereas the effusivity and the thermal diffusivity of the coatings are not sufficiently sensitive to the transition from Zone I to Zone II, and - (ii) this combined thermal coating parameter (16) is determined as a function of the two parameters  $(e_c/e_b)$  and  $\tau_c$ , which can directly be measured by Modulated IR Radiometry. This means, the gas mixture flow and the resulting crystalline structure can directly be monitored with the help of the combined parameter  $[d_c(\rho \cdot c)_c]$ , determined as a function of the value of the relative phase extremum and of its modulation frequency  $\{\Phi_{n \text{ extr}}, f_{\text{extr}}\}$ .

## 5. Determination of the Coating Thickness by means of Modulated IR Radiometry

In order to determine the film thickness by means of Modulated IR Radiometry, different sets of TiCO thin films have been prepared keeping constant the deposition parameters, except the deposition time, in order to obtain thin films of approximately equal composition, structure, and equal thermal transport properties, but different film thickness. The results obtained by Modulated IR Radiometry are compared with the coating thickness determined by destructive measurements, in order to analyze the reliability, the error limits, and the main limitations of non-contact non-destructive Modulated IR Radiometry, when applied to sputter-deposited thin films and coatings. Compared to former work on the coating thickness of varnish layers [20], higher heating modulation frequencies have to be used in the present work, to determine the coating thickness and thus it is possible to visualize the limitations of Modulated IR Radiometry.

Based on the definition of the thermal diffusion time of the coating (6) and on the inverse solution for the thermal diffusion time (13) as a function of the measured relative extremum, the coating thickness can be determined as

$$d_c = \sqrt{\alpha_c \cdot \tau_c} = \sqrt{\alpha_c} \cdot \frac{1}{4\sqrt{\pi f_{\text{extr}}}} \cos^{-1}[(\tan \Phi_{n \text{ extr}})^2] \quad (20)$$

with  $\alpha_c = k_c/(\rho \cdot c)_c$  the thermal diffusivity of the coating, and  $\Phi_{n \text{ extr}}$  and  $f_{\text{extr}}$  the values measured for the relative extremum. The effects of crystallization or crystalline disorder and meso- or macroscopic porosity in general affect the thermal conductivity  $k_c$  and the volume heat capacity  $(\rho \cdot c)_c$  similarly [21] and thus accumulate in the thermal effusivity  $\sqrt{k_c(\rho \cdot c)_c}$ , whereas they can partially eliminate each other in the thermal diffusivity  $\alpha_c = k_c/(\rho \cdot c)_c$ . Assuming that the thermal transport properties remain approximately constant during the

deposition process, an assumption which can be monitored by the value for the measured phase extremum  $\Phi_{n \text{ extr}}$ , directly related according to equ.(12) and (14) to the thermal effusivity

$$\frac{e_c}{e_b} = \frac{\sqrt{1 + \tan\{0.5 \cos^{-1}[(\tan \Phi_{n \text{ extr}})^2]\}} - \sqrt{1 - \tan\{0.5 \cos^{-1}[(\tan \Phi_{n \text{ extr}})^2]\}} \cdot \exp\{0.5 \cos^{-1}[(\tan \Phi_{n \text{ extr}})^2]\}}{\sqrt{1 + \tan\{0.5 \cos^{-1}[(\tan \Phi_{n \text{ extr}})^2]\}} + \sqrt{1 - \tan\{0.5 \cos^{-1}[(\tan \Phi_{n \text{ extr}})^2]\}} \cdot \exp\{0.5 \cos^{-1}[(\tan \Phi_{n \text{ extr}})^2]\}} \quad (21)$$

we can assume that the thermal diffusivity remains approximately constant,  $\alpha_c \approx \alpha_{c0}$ , and that equ.(20) can be simplified to

$$d_c = \sqrt{\alpha_{c0}} \cdot \sqrt{\tau_c (f_{\text{extr}}, \Phi_{n \text{ extr}})} = \sqrt{\alpha_{c0}} \cdot \frac{1}{4\sqrt{\pi f_{\text{extr}}}} \cos^{-1}[(\tan \Phi_{n \text{ extr}})^2] \quad (20a)$$

When the coating thickness is determined for a set of coatings deposited at constant deposition conditions – which means, for coatings of approximately equal effusivity controlled with the help of equ.(21) – independent thickness measurements by a microscopic measurement method [5,22] are required, which are used for the thickness calibration of the set of coatings. Effects of surface roughness or thin surface layers of different thermal properties on top of the coating and effects of semi-transparency in the visible and IR spectrum affect the signals measured for thinner coatings more than the signals measured for thicker coatings. Consequently, thicker coatings without effects of semi-transparency and without surface layers of different thermal transport properties are preferentially used for the thickness calibration.

In Fig. 8 the inverse calibrated phase lag signals are shown, which have been measured for a set of Titanium-Oxy-Carbide thin films deposited by reactive magnetron sputtering on tool steel. The measured data are approximated by solutions of the opaque two-layer model (8), and the thermal parameters  $R_{cb}$  (12) and  $\tau_c$  (13) are calculated using the values  $\{\Phi_{n \text{ extr}}, f_{\text{extr}}\}$  measured for the relative minima in the range of intermediate modulation frequencies,  $50 < (f/\text{Hz})^{1/2} < 125$ .

The deviations between theoretical approximation and measured data at low modulation frequencies,  $0 < (f/\text{Hz})^{1/2} < 25$ , corresponding to large thermal penetration depths, are related to the effects of substrate pre-treatment and heat propagation in the substrate [8,12], whereas the deviations at higher heating modulation frequencies,  $(f/\text{Hz})^{1/2} > 150$ , corresponding to short thermal penetration depths, are related to coatings with additional thin surface layers  $\{\text{TiCO(D2)}, \text{TiCO(D4)}\}$  with the thermal effusivity differing due to surface roughness [10,11] from that of the coating as a whole,  $e_s < e_c$ . The deviations between theoretical approximation and measured data of the coating TiCO(D1) at high modulation frequencies are related to the effects of semi-transparency.

Using one of the thicker coatings in Fig.8 for the thickness calibration, namely coating TiCO(D3  $\diamond$ ), which shows good agreement between measured data and opaque two-layer model at intermediate and higher modulation frequencies, the thermal diffusivity of this set of coatings can be determined as  $\alpha_{c0} = d_{c \text{ micro}}^2 / \tau_{c \text{ MIRR}} = 2.5 \cdot 10^{-6} \text{ m}^2/\text{s}$ , with  $d_{c \text{ micro}}$  the reference coating thickness determined by the microscopic destructive measurement and the thermal diffusion time determined by non-contact non-destructive Modulated IR Radiometry (MIRR). The thickness of the other coatings can then be determined according to equ. (20a).

Comparing the values of the coating thickness  $d_{c \text{ MIRR}} = (\alpha_{c0} \cdot \tau_c)^{1/2}$  obtained by Modulated IR Radiometry (Table 2a) with the values  $d_{c \text{ micro}}$  measured by the microscopic destructive method - ball cratering based on the CALOTEST device [5] - relative errors

$$\frac{\Delta d_c}{d_c} = \frac{d_{c \text{ MIRR}} - d_{c \text{ micro}}}{d_{c \text{ micro}}} \quad (22)$$

for  $d_{c \text{ MIRR}}$  of about 3.9%, 3.3%, and 1.4% are obtained, and the average error of the thickness measurements by *Modulated IR Radiometry* results as about 3%.

If the thickest coating TiCO(D4 x) of the set of coatings in Fig. 8 is used for the calibration of the thickness measurements based on Modulated IR Radiometry (Table 2.b), a slightly lower value of  $\alpha_{c 0} = d_{c \text{ micro}}^2/\tau_c = 2.44 \cdot 10^{-6} \text{ m}^2/\text{s}$  is obtained for the effective thermal diffusivity and slightly lower values are also obtained for the coating thickness  $d_{c \text{ MIRR}}$  determined by Modulated IR Radiometry, as well as a slightly lower averaged value for the relative errors (Table 2b).

These rather stable results are due to the fact that both the thermal transport properties and the coating thickness determined by non-contact non-destructive Modulated IR Radiometry are based on thermal wave data (Fig. 3, Fig. 8), measured at intermediate modulation frequencies,  $55 < (f/\text{Hz})^{1/2} < 115$ , far from  $1/f$  - noise at low modulation frequencies and far from the effects of IR background fluctuations at high modulation frequencies (Fig. 9). At the intermediate modulation frequencies, where the relative phase extrema are found, the measured thermal wave amplitudes (Fig. 10) are still rather large, e.g.  $S \approx 1.25 \text{ mV}$  for the coated sample TiCO (E4 x), corresponding to a thermal wave amplitude of about  $\delta T \approx 660 \text{ } \mu\text{K}$ , and  $S \approx 0.6 \text{ mV}$  for the coated samples TiCO (D4 \*) and TiCO (E3 Δ), corresponding to thermal wave amplitudes of about  $\delta T \approx 320 \text{ } \mu\text{K}$ , compared to the detection limit [7] of about  $\delta T \approx 44 \text{ } \mu\text{K}$ , imposed by the incoherent IR background fluctuations at 300 K.

In order to discuss the principal limitations of the non-contact non-destructive method of thickness measurements, the inverse calibrated phase lag signals measured for the second set of titanium oxycarbide coatings, prepared at different deposition conditions with an approximately constant, but lower coating effusivity ( $e_c/e_b$ ) $\approx 0.317$ , are compared with opaque two-layer approximations in Fig. 9.

For one of the thicker coatings of this set of samples, namely TiCO(E3 Δ), there is again a rather good agreement between measured data and opaque two-layer model in the range of the intermediate heating modulation frequencies,  $45 < (f/\text{Hz})^{1/2} < 200$ , describing the coating properties. Thus, this coating with its thickness of  $d_{c \text{ micro}}=2.47 \text{ } \mu\text{m}$  determined by the destructive microscopic measurement is used for the thickness calibration (Table 3a). Using the thermal diffusivity of  $\alpha_{c 0} = d_{c \text{ micro}}^2/\tau_c = 1.024 \cdot 10^{-6} \text{ m}^2/\text{s}$  resulting for this reference coating, the thickness of the other coatings can again be determined according to equ.(20a). When comparing the resulting values of coating thickness obtained by *Modulated IR Radiometry* with the values measured by the microscopic destructive method [5], one can see, that the error of measurement is about 14% in the case of the thickest coating TiCO(E4 x), whereas the relative errors of the two measurements TiCO(E1 ϖ) and TiCO(E2 ♦) on the thin coating are much larger, -52% and -63% respectively (Table 3a).

If on the other hand the thickest coating TiCO(E4 x) is here used for the thickness calibration, similar to the thickness calibration in Table 2b, the relative errors of the coating thickness measurements based on Modulated IR Radiometry get even larger (Table 3b). The very large relative errors found in Table 3a and Table 3b for the two measurements {TiCO(E1 ϖ), TiCO(E2 ♦)} on the thin coating are due to the fact that the measured amplitude signals (Fig. 10), which decrease with increasing modulation frequency, get very small and are already affected by IR background fluctuations [7] and that only small deviations measured for the inverse calibrated phase lag signals  $\Phi_n(f)$  can already lead to large shifts of the modulation frequency  $f_{\text{extr}}$  of the relative extremum  $\Phi_{n \text{ extr}}$ . This can be seen in Fig. 9 for the data obtained in repeated measurements on the thin coating, where small deviations of the measured data (ϖ, ♦) from the two-layer approximations are observed above about  $(f/\text{Hz})^{1/2} > 150$ .

For the thickest coating TiCO(E4  $\times$ ) of this set of coatings with its relative minimum at about  $(f_{\text{extr}}/\text{Hz})^{1/2} \approx 57$  (Fig. 9), there are considerable systematic deviations between the opaque two-layer model (- - -) and the data ( $\times$ ) measured at higher modulation frequencies,  $(f/\text{Hz})^{1/2} > 120$ . In principle, such deviations can be due to a thin surface layer of higher effusivity,  $e_s > e_c$ , on top of the coating or due to a semi-transparent surface layer. Similarly, there are small deviations between the data measured for coating TiCO(E3  $\Delta$ ) and the opaque two-layer model (—) systematically increasing above about  $(f/\text{Hz})^{1/2} > 225$ . The large deviations between measured data and opaque two-layer model observed for coating TiCO(E4  $\times$ ) and the smaller deviations observed for coating TiCO(E3  $\Delta$ ) in Fig. 9 are related to the semi-transparency in the IR spectrum, correlating with the higher carbon content and the lower thermal effusivity of this set of coatings. The relative errors of about 12% and 14% in Table 3a and Table 3b for the two thicker coatings are thus not errors of measurement but errors related to the theoretical model used for the quantitative interpretation of the measured data: - Instead of an opaque two-layer model, a two-layer model allowing contributions to the detected signal based on IR emission from below the coating surface should be used. Such signal contributions should also exist in the two measurements {TiCO(E1  $\diamond$ ), TiCO(E2  $\blacklozenge$ )} on the thin coating, can however not be identified in Fig. 9 due to the limited range of heating modulation frequencies,  $(f/\text{Hz})^{1/2} \leq 325$ , accessible to measurement and due to the IR background fluctuations limiting a reliable detection for thinner coatings already in the range of  $(f/\text{Hz})^{1/2} > 150$ .

## 6. Conclusions and Outlook

Modulated IR Radiometry (MIRR), a non-destructive non-contact measurement technique based on the excitation of thermal waves by modulated laser beam heating and on the IR detection of the thermal wave response, has been shown to be a useful tool for the control of coatings and their deposition processes.

For the quantitative interpretation of the measured signals, preferentially the thermal waves' phase lag signals relative to the heating modulation are used, since these signals depend on a minor number of physical parameters than the thermal waves' amplitude signals. Based on a mathematical unique solution for the two-layer thermal wave problem, the thermal coating parameters have been determined as physically reliable solutions for coating-substrate systems. Directly measurable quantities, which are determined as a function of the relative extrema of the inverse calibrated phase lag signals, i.e. of the value of the relative extremum and of the modulation frequency, where the relative extremum is localized, are the ratio of the thermal effusivities coating-to-substrate and the coatings' thermal diffusion time, which are the relevant thermal coating parameters for time-dependent heating processes of coatings. Apart from the directly measurable thermal quantities, there are also combined thermal quantities, e.g. the *surface area heat capacity* of coatings, which e.g. gives information about the heat insulation properties of coated cutting tools.

In measurements on different sputter-deposited coatings, e.g. ZrON and TiCO coatings in the present work, it has been found that the coatings' effusivity directly correlates with the deposition conditions, e.g. the gas mixture flow, and that based on the coatings' thermal effusivity the deposition conditions can thus be monitored by non-contact non-destructive Modulated IR Radiometry. Based on the results obtained by Modulated IR Radiometry for the thermal coating properties, a "rule of thumb" may be applied to check whether a new developed coating may be appropriate or not for certain applications, where heat generation and surface heating processes play a dominant role and where the thermal transport properties of the coatings are thus of crucial importance, e.g. on coated cutting tools.

In addition it has been found, that the coating thickness can be monitored in deposition processes done under constant deposition conditions. For this latter application, the control of

the coating thickness, the principal limitations and error limits have been analyzed: - (1) For thinner coatings, the main limitation is given by the device-dependent limitation of the range of heating modulation frequencies, accessible to measurement at higher frequencies. - (2) This device-dependent limitation at high heating modulation frequencies additionally can be shifted to lower heating modulation frequencies by fluctuations of the IR background, leading to smaller errors of the measured phase lag signals and to larger errors of the heating modulation frequencies, where the relative extrema of the inverse calibrated phase lag signals are localized. - (3) Both for thinner and thicker coatings, the deviations of real coatings from the opaque two-layer model used for the quantitative interpretation of the measurements can contribute to larger errors. In general, such deviations can be related to semi-transparency both in the visible and the IR spectrum, and to additional thin surface layers, with the effusivity differing from that of the coating.

The control of the film thickness opens a wide range of possible applications, which may include the film thickness evaluation during the deposition process, the life-time of thin films and their thickness reduction on industrial coated tools. Thermal wave excitation and detection which has already been applied on limiter and divertor plates used in nuclear fusion devices [16] to analyze the effects of erosion and material re-deposition, may also be a useful tool for the in-situ control of the Tritium content [23] in limiters, divertor plates, and vessel walls, when Modulated IR Radiometry is applied for the thermal wave excitation and detection.

### Acknowledgements

This research has been done in the frame of the cooperation between Ruhr-University Bochum and University of Minho Braga - Guimarães, in part supported by DAAD (Germany) and GRICES (Portugal). Part of this research was sponsored by FEDER funds through the program COMPETE-Programa Operacional Factores de Competitividade and by national funds through FCT-Fundação para a Ciência e a Tecnologia, under the project PTDC/CTM/69362/2006. One of the authors, R. Faria Jr., would like to thank CAPES (Coordenação de Aperfeiçoamento de Pessoal, Brazil) for financial support.

### REFERENCES

- [1] E.L. Toth, *Transition Metal Carbides and Nitrides*, Academic Press, New York, 1971.
- [2] B.W. Allcock, P.A. Lavin, *Novel composite coating technology in primary and conversion industry applications*, Surf. Coat. Technol. 163-164 (2003) 62–66.
- [3] P. Carvalho, F. Vaz, L. Rebouta, L. Cunha, C. J. Tavares, C. Moura, E. Alves, A. Cavaleiro, Ph. Goudeau, E. Le Bourhis, J. P. Rivière, J. F. Pierson, O. Banakh, *Structural, electrical, optical, and mechanical characterizations of decorative  $ZrO_xN_y$  thin films*, J. Appl. Phys. 98 (2005) 023715.
- [4] P. Carvalho, J.M. Chappé, L. Cunha, S. Lanceros-Méndez, P. Alpuim, F. Vaz, E. Alves, C. Rousselot, J.P. Espinós, A.R. González-Elipse, *Influence of the chemical and electronic structure on the electrical behavior of zirconium oxynitride films*, J. Appl. Phys. 103 (2008) 104907.
- [5] CALOTEST® equipment, CSM Instruments, Switzerland.
- [6] Th. Orth, W. Fluegge, J. Gibkes, *Characterisation of organic thin film coatings on automobile steel sheets by photothermal methods*, 9th Europ.Conf.on NDT, Sept.25-29, 2006, Berlin, publ. in: Conf.Proc. EC NDT Berlin 2006.
- [7] J. Bolte, J.H. Gu, B.K. Bein, *Background fluctuation limit of IR detection of thermal waves at high temperatures*, High Temp.- High Pressures 29 (1997) 567-580.
- [8] F. Macedo, J. Ferreira, F. Vaz, L. Rebouta, A. Haj Daoud, D. Dietzel, B.K. Bein, *Photothermal characterization of sputtered thin films and substrate treatment*, Photoacoustic

- & Photothermal Phenomena (eds. F. Scudieri a. M. Bertolotti), AIP Conf. Proc. 463 (1999) 536-538.
- [9] C.A. Bennett, R.R. Patty, *Thermal wave interferometry: a potential application of the photoacoustic effect*, Appl. Optics 21 (1982) 49–54.
- [10] F. Macedo, F. Vaz, L. Rebouta, P. Carvalho, A. Haj-Daoud, K.H. Junge, J. Pelzl, B.K. Bein, *Modulated IR radiometry of (TiSi)N thin films*, Vacuum 82 (2008) 1457–1460.
- [11] H.G. Walther, *Surface roughness influence on photothermal radiometry*, Appl. Surf. Sci. 193, 1-4 (2002) 156.
- [12] J.L. Nzodoum Fotsing, B.K. Bein, J. Pelzl, *Potentialities of photothermal displacement experiments in micro-scaled systems*, Superlattices and Microstructures 35 (2004), 419-435 (Elsevier Science), Proceed. Microscale Heat Transfer, Eurotherm Sem. 75, Reims, July 8-10, 2003.
- [13] J.L. Nzodoum Fotsing, J. Gibkes, J. Pelzl, B.K. Bein, *Extremum method: Inverse solution of the two-layer thermal wave problem*, J. Appl. Phys. 98 (2005), 063522.
- [14] J.L. Nzodoum Fotsing, *Friction wear of coatings analyzed by means of thermal wave excitation and modulated IR radiometry*, Wear 264, Issue 1-2 (Jan.2008) 119-130; Publ. online Wear 25.4.2007, DOI:10.1016/j.wear.2007.03.017.Wear.
- [15] H.S. Carslaw and J.C. Jaeger, (1984), *Conduction of Heat in Solids*, Oxford University Press, London (1984).
- [16] B.K. Bein and J. Pelzl, *Analysis of Surfaces Exposed to Plasmas by Nondestructive Photoacoustic and Photothermal Techniques*, Plasma Diagnostics, Vol. 2, Surface Analysis and Interactions, (Eds. O. Auciello, D.L. Flamm), Academic Press, 1989, 211-326.
- [17] E.R. Müller, B.K. Bein, K. Steinmetz, *Time and space-resolved energy flux measurements in the divertor of the ASDEX Tokamak by computerized IR thermography*, Report IPP III/97, Max-Planck-Institut für Plasmaphysik, Garching, Germany, (1984).
- [18] H. Würz, B.K. Bein, J. Neuhauser, D. Zasche, *Power flow to the ASDEX divertor plates*, Fusion Technology 1988, Vol. 1, (Eds. A.M. van Ingen, A. Nijsen-Vis, H.T. Klippel, North Holland, Elsevier Science Publ., Amsterdam, 1989), 867-873.
- [19] F. Macedo, P. Carvalho, L. Cunha, F. Vaz, J. Gibkes, B.K. Bein, J. Pelzl, *The role of modulated IR radiometry measurements in the characterization of Zr-O-N thin films*, Plasma Process. Polym. 6, (2009), S760-S766.
- [20] M. Chirtoc, J. Gibkes, H.G. Walther, A. Christ, J.S. Antoniow, D. Bicanic, Z. Bozoki, G. Szabo, B. Bein, J. Pelzl, M. Kleebauer, H. Bader, a. M. Marinelli, *Comparative study of coating thickness determination in packaging composite materials using photothermal radiometry, photoacoustic and photopyroelectric methods*, Analytical Sciences 17 (2001), s185-s188 (Special Issue), Ed. The Japan Society for Analytical Chemistry.
- [21] M. E. Cunningham and K. L. Peddicord, *Heat conduction in spheres packed in an infinite regular cubical array*, Int. Heat Mass Transfer 24 (1981) 1081-1088.
- [22] F. Macedo, F. Vaz, A.C. Fernandes, J.L. Nzodoum-Fotsing, J. Gibkes, J. Pelzl, B.K. Bein, *Thickness control of coatings by means of modulated IR radiometry*, Plasma Process. Polym. 6, (2009), S592-S598.
- [23] A. Nicolai, P. Börner, *Minimization of the Tritium content within the first wall of a Tokamak reactor*, Fusion Technology 12 (1987) 119.

## Tables

**Table 1**

**Table 1.** Deposition conditions, resulting atomic concentration ratios, measured relative extrema, and effective thermal coating parameters for a set of ZrON thin films on tool steel.

Thin ZrON films	(N <sub>2</sub> +O <sub>2</sub> ) gas flow [sccm]	(C <sub>N</sub> +C <sub>O</sub> )/C <sub>Zr</sub>	(f/Hz) <sub>extr</sub> <sup>1/2</sup>	Φ <sub>n extr</sub> [deg]	(e <sub>c</sub> /e <sub>b</sub> )	τ <sub>c</sub> [μs]	[d <sub>c</sub> (ρc)] <sub>c</sub> [J/(m <sup>2</sup> K)]	d <sub>c</sub> [μm]	α <sub>c</sub> [m <sup>2</sup> /s]
ZrON1	8.5	1.29	64	-16.3	0.39	10.7	10.85	3.666	1.3 10 <sup>-6</sup>
ZrON2	9	1.30	64	-16.3	0.39	10.7	10.83	3.337	1.0 10 <sup>-6</sup>
ZrON5	10	1.35	64	-18.2	0.35	10.4	9.44	3.522	1.2 10 <sup>-6</sup>
ZrON6	11	1.38	64	-19.5	0.32	10.1	8.54	2.983	8.8 10 <sup>-7</sup>
ZrON7	12.5	1.46	57	-21.7	0.27	12.2	8.01	2.888	6.8 10 <sup>-7</sup>
ZrON8	13.5	1.45	64	-20.9	0.29	9.86	7.64	2.618	7.0 10 <sup>-7</sup>
ZrON9	15	1.45	51	-22.2	0.26	15.1	8.55	3.159	6.6 10 <sup>-7</sup>
ZrON3	16	1.49	57	-21.2	0.28	12.4	8.38	2.710	5.9 10 <sup>-7</sup>
ZrON4	17.5	1.50	57	-20.1	0.31	12.5	9.13	2.585	5.3 10 <sup>-7</sup>

**Table 2a**

**Table 2a** Measured *relative phase extrema* and thermal coating parameters for a set of titanium oxycarbide coatings of approximately equal thermal transport properties and different values of the coating thickness, determined by Modulated IR radiometry (MIRR) and destructive thickness measurements (ball cratering).

Coating	(f <sub>min</sub> /Hz) <sup>1/2</sup>	Φ <sub>n min</sub> [deg]	R <sub>cb</sub>	(e <sub>c</sub> /e <sub>b</sub> )	τ <sub>c</sub> [10 <sup>-6</sup> s]	α <sub>c 0</sub> [10 <sup>-6</sup> m <sup>2</sup> /s]	d <sub>c MIRR</sub> [μm]	d <sub>c micro</sub> [μm]	$\frac{\Delta d_c}{d_c}$
TiCO(D1 Δ)	113.87	-16.14	-0.431	0.40	3.39		2.91	2.8	3.9%
TiCO(D2 □)	66.30	-16.10	-0.430	0.40	10.01		5.00	4.84	3.3%
TiCO(D3 ◇)	64.13	-15.33	-0.410	0.42	10.82	2.50	5.2	5.2	
TiCO(D4 x)	57.01	-14.19	-0.380	0.45	13.9		5.90	5.82	1.4%

**Table 2b**

**Table 2b.** Measured *relative phase extrema* and thermal coating parameters of a set of titanium oxycarbide coatings of approximately equal thermal transport properties and different values of the coating thickness, determined by MIRR and destructive thickness measurements.

Coating	(f <sub>min</sub> /Hz) <sup>1/2</sup>	Φ <sub>n min</sub> [deg]	R <sub>cb</sub>	(e <sub>c</sub> /e <sub>b</sub> )	τ <sub>c</sub> [10 <sup>-6</sup> s]	α <sub>c 0</sub> [10 <sup>-6</sup> m <sup>2</sup> /s]	d <sub>c MIRR</sub> [μm]	d <sub>c micro</sub> [μm]	$\frac{\Delta d_c}{d_c}$
TiCO(D1 Δ)	113.87	-16.14	-0.431	0.40	3.39		2.88	2.8	+2.9%
TiCO(D2 □)	66.30	-16.10	-0.430	0.40	10.01		4.94	4.84	+2.1%
TiCO(D3 ◇)	64.13	-15.33	-0.410	0.42	10.8		5.13	5.2	-1.3%
TiCO(D4 x)	57.01	-14.19	-0.380	0.45	13.9	2.44	5.82	5.82	

**Table 3a**

**Table 3a.** Measured *relative phase extrema* and thermal coating parameters of a set of titanium oxycarbide coatings of approximately constant but lower thermal transport properties – with larger deviations between the coating thicknesses determined by MIRR and the values obtained by destructive thickness measurements.

Coating	(f <sub>min</sub> /Hz) <sup>1/2</sup>	Φ <sub>n min</sub> [deg]	R <sub>cb</sub>	(e <sub>c</sub> /e <sub>b</sub> )	τ <sub>c</sub> [10 <sup>-6</sup> s]	α <sub>c 0</sub> [10 <sup>-6</sup> m <sup>2</sup> /s]	d <sub>c MIRR</sub> [μm]	d <sub>c micro</sub> [μm]	$\frac{\Delta d_c}{d_c}$
TiCO(E1 ◇)	287.35	-20.04	-0.530	0.307	0.498		0.71	1.91	-62.8%
TiCO(E2 ◆)	227.60	-19.05	-0.505	0.329	0.809		0.91	1.91	-52.4%
TiCO(E3 Δ)	83.42	-19.62	-0.520	0.316	5.956	1.024	2.47	2.47	
TiCO(E4 x)	57.01	-19.81	-0.525	0.312	12.706		3.61	3.16	+14.2%

**Table 3b**

**Table 3b.** Measured *relative phase extrema* and thermal coating parameters of a set of titanium oxycarbide coatings of approximately constant but lower thermal transport properties – with larger deviations between the coating thicknesses determined by MIRR and the values obtained by destructive measurements.

<b>Coating</b>	$(f_{\min}/\text{Hz})^{1/2}$	$\Phi_{n \min}$ [deg]	$R_{cb}$	$(e_c/e_b)$	$\tau_c$ [ $10^{-6}$ s]	$\alpha_{c0}$ [ $10^{-6}$ m <sup>2</sup> /s]	$d_{c \text{ MIRR}}$ [ $\mu\text{m}$ ]	$d_{c \text{ micro}}$ [ $\mu\text{m}$ ]	$\frac{\Delta d_c}{d_c}$
TiCO(E1 $\diamond$ )	287.35	-20.04	-0.530	0.307	0.498		0.63	1.91	-67.0%
TiCO(E2 $\blacklozenge$ )	227.60	-19.05	-0.505	0.329	0.809		0.80	1.91	-58.1%
TiCO(E3 $\Delta$ )	83.42	-19.62	-0.520	0.316	5.956		2.16	2.47	-12.6%
TiCO(E4 $\times$ )	57.01	-19.81	-0.525	0.312	12.706	0.786	3.16	3.16	

## Figures captions

**Figure 1.** Schematic of the measurement system used for Modulated IR Radiometry.

**Figure 2.** Inverse calibrated modulated IR amplitudes measured for some examples of ZrON coatings on tool steel (ZrON1, ZrON2, ZrON3, ZrON4), represented as a function of  $f^{-1/2}$ , proportional to the thermal waves penetration depth of  $x_{th} \propto f^{-1/2}$ .

**Figure 3.** Inverse calibrated modulated IR phases measured as a function of modulation frequency for various sputter deposited coatings (ZrON1, ZrON2, ZrON3, ZrON4) on tool steel, represented as a function of  $(f/\text{Hz})^{1/2}$ .

**Figure 4.** Correlation between the values of the relative extrema of the inverse calibrated phase lag signals and the gas mixture flow used for the deposition of a set of ZrON thin films.

**Figure 5:** Ratio of the effusivities ( $e_c/e_b$ ) coating-to-substrate of ZrON thin films as a function of the atomic concentration ratio  $(C_N+C_O)/C_{Zr}$ .

**Figure 6.** Thermal diffusivity  $\alpha_c = k_c/(\rho_c \cdot c_c)$  of the ZrON thin films as a function of the atomic concentration ratio  $(C_N+C_O)/C_{Zr}$ .

**Figure 7.** *Surface area heat capacity* [ $d_c(\rho \cdot c)_c$ ] giving information on the coatings' heat insulation properties, as a function of the gas mixture (95% N<sub>2</sub>+ 5% O<sub>2</sub>) flow during deposition.

**Figure 8.** Inverse calibrated IR phase lag signals measured for titanium oxycarbide coatings {TiCO(D1  $\Delta$ ), TiCO(D2  $\square$ ), TiCO(D3  $\diamond$ ), TiCO(D4  $\times$ )} of approximately equal thermal effusivity on high speed steel (AISI M2), in comparison with opaque two-layer approximations.

**Figure 9.** Inverse calibrated IR phase lag signals of a set of titanium oxycarbide coatings {TiCO(E1  $\diamond$ ), TiCO(E2  $\blacklozenge$ ), TiCO(E3  $\Delta$ ), TiCO(E4  $\times$ )} of approximately constant, but lower effusivity, compared to opaque two-layer approximations. – The data TiCO(E1  $\diamond$ ) and TiCO(E2  $\blacklozenge$ ) were measured at different positions on the same coating.

**Figure 10.** Amplitude signals measured by Modulated IR Radiometry for thinner and thicker coatings on tool steel of two different sets of coatings {TiCO(E1  $\diamond$ ), TiCO(E3  $\Delta$ ), TiCO(E4  $\times$ )} and {TiCO(D1  $\blacktriangleleft$ ), TiCO(D4  $*$ )} and for the homogeneous opaque reference sample of smooth surface (Glassy carbon Sigradur  $\blacksquare$ ), used for the calibration of the signals measured for the two sets of coatings (Comp. Sect. 3).

Figure 1

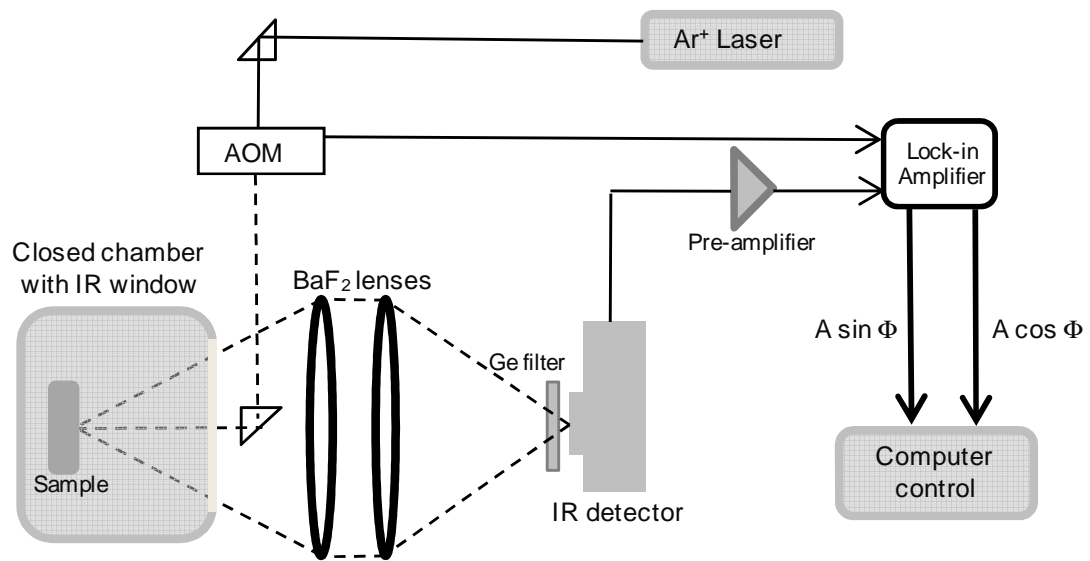


Figure 2

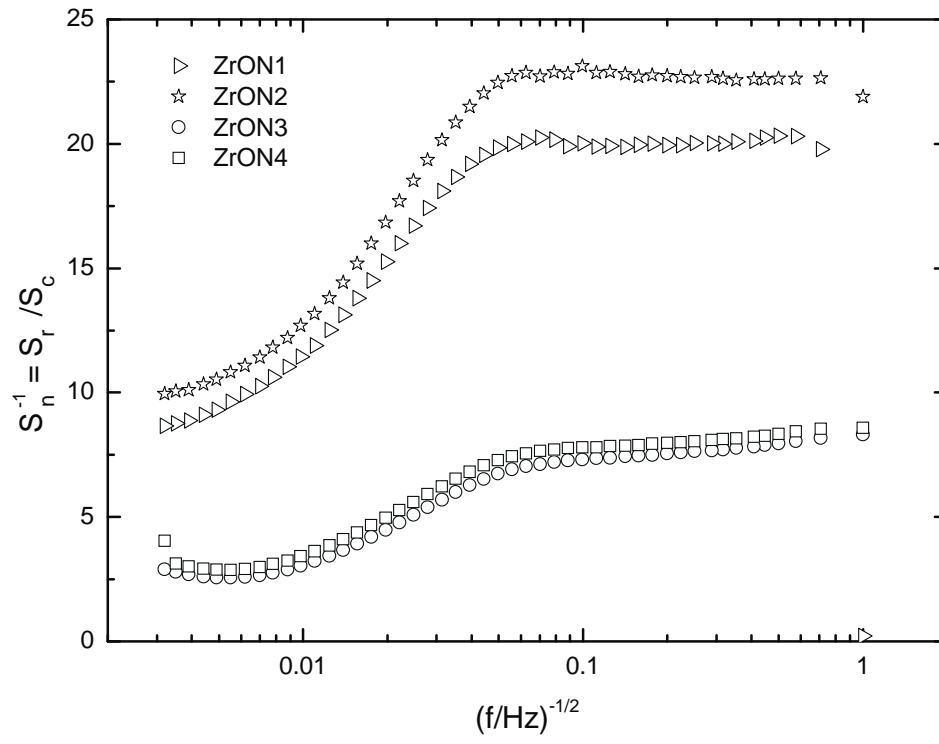


Figure 3

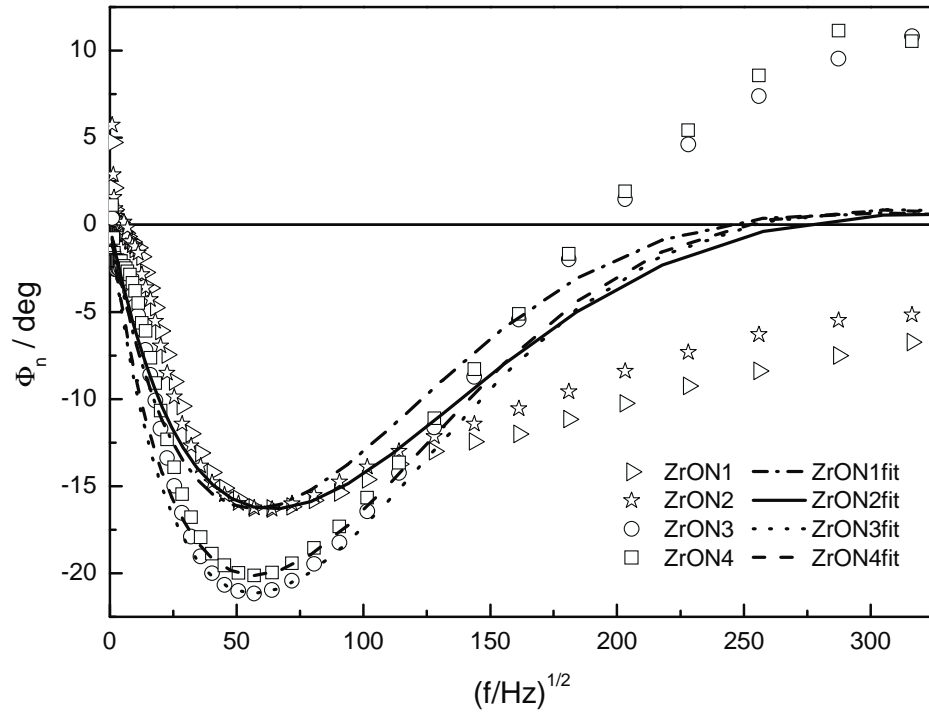


Figure 4

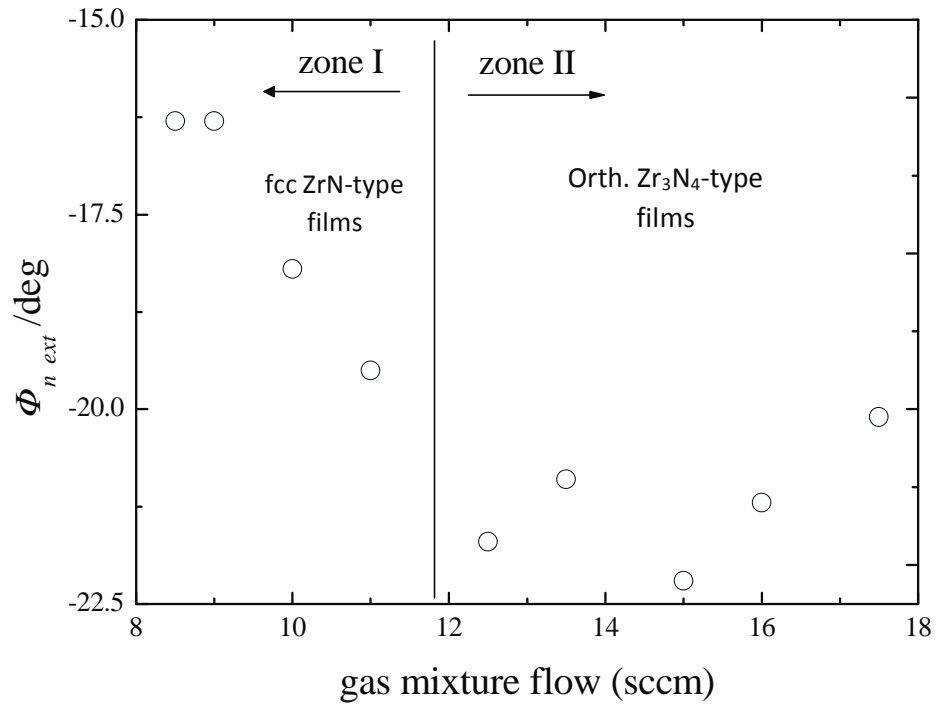


Figure 5

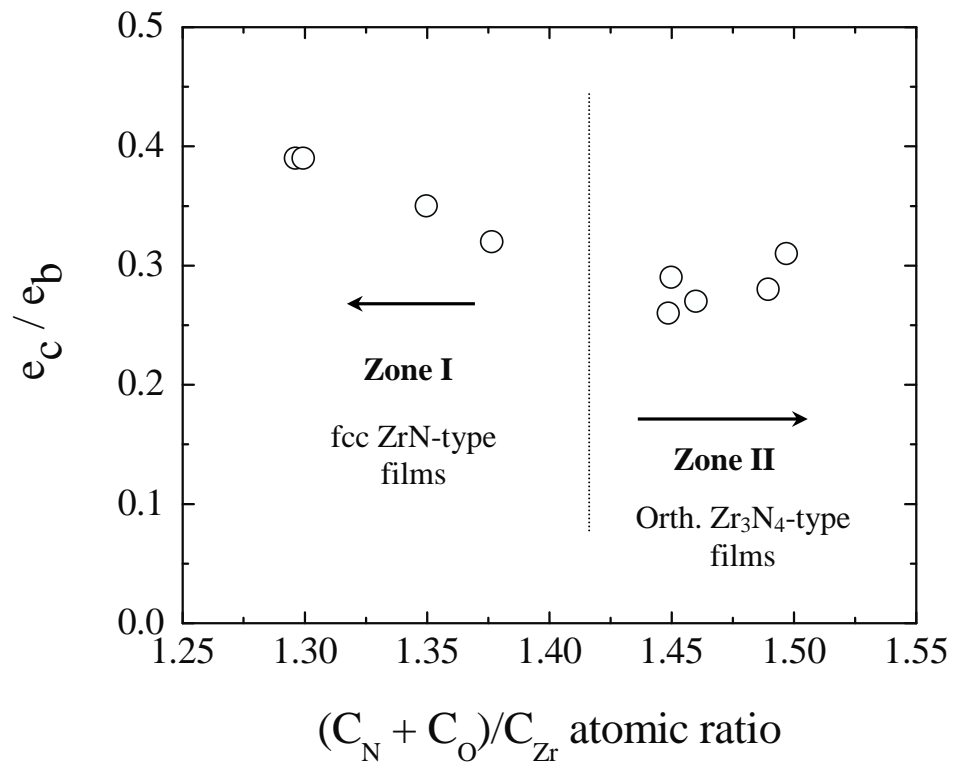
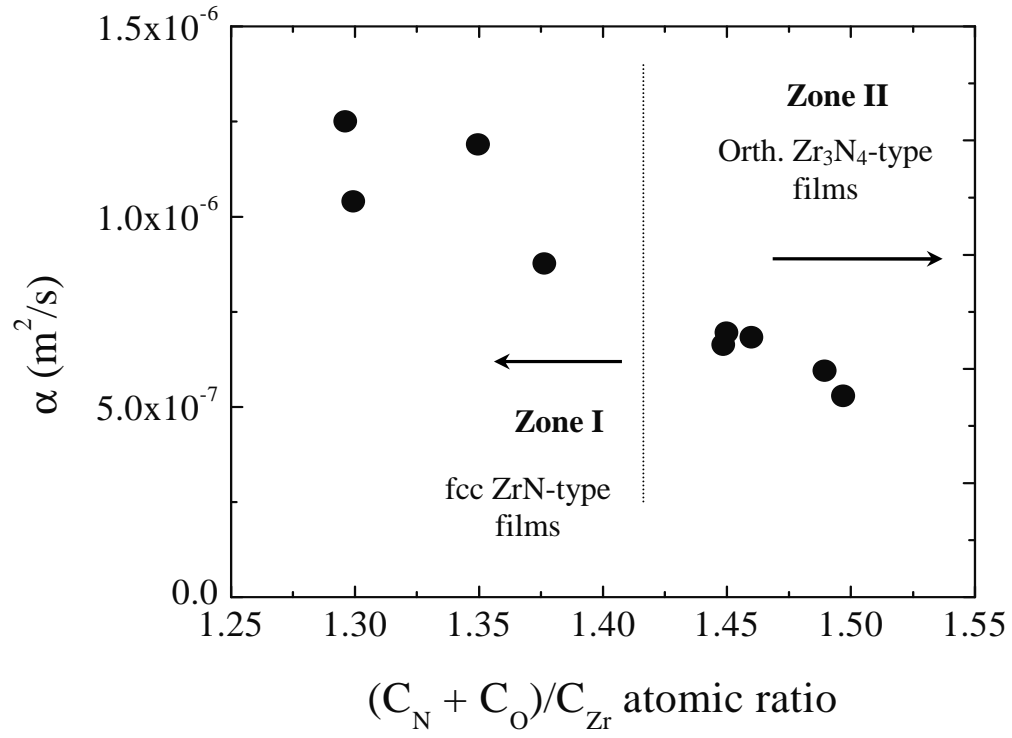


Figure 6



**Figure 7**

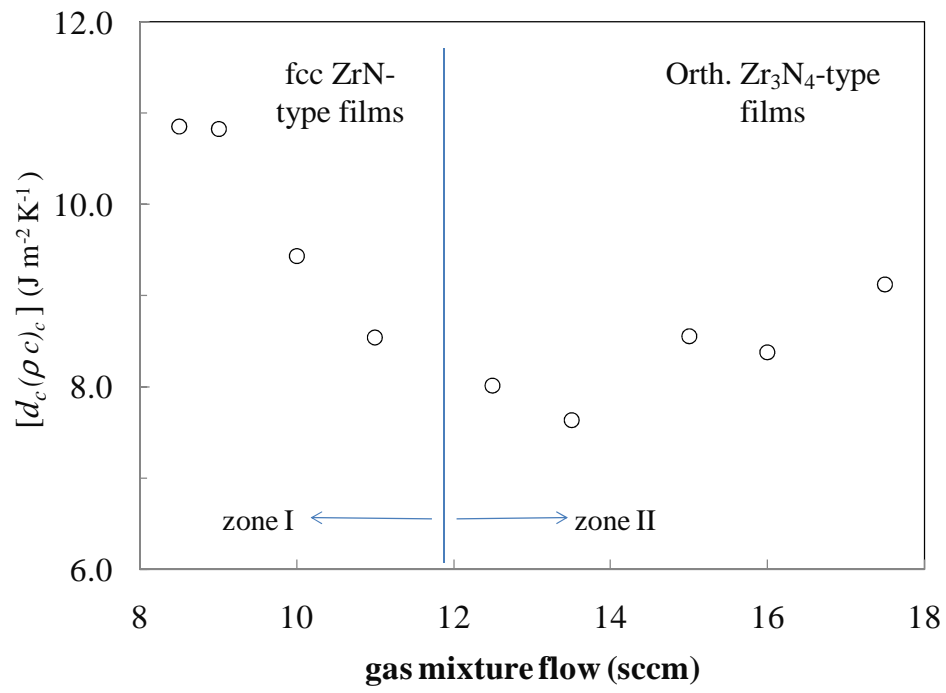


Figure 8

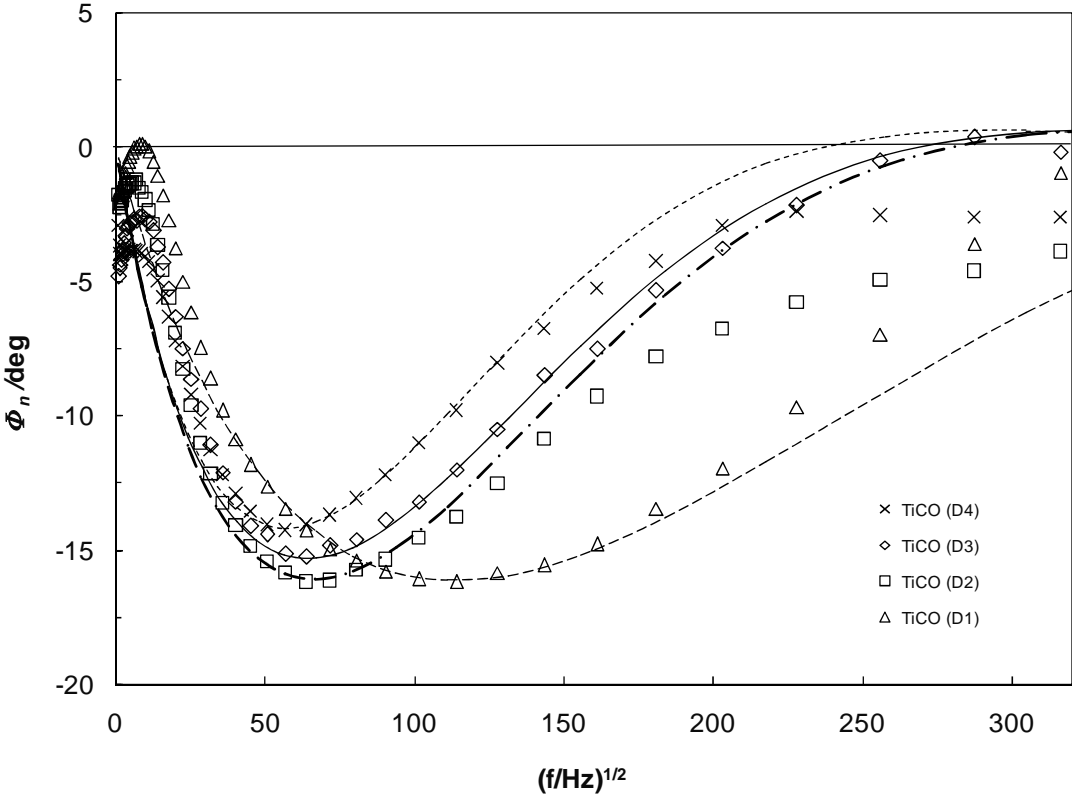


Figure 9

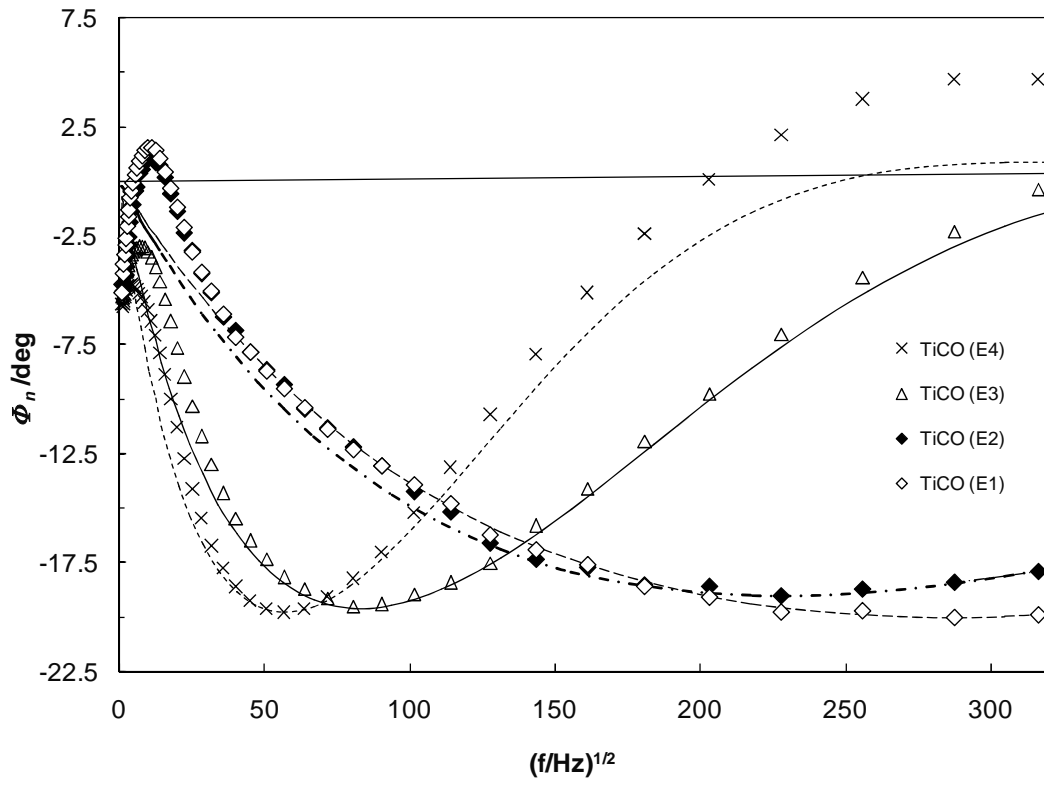


Figure 10

